

## Supporting Information

### **Novel COF@Ti-MOF hybrid photocatalysts enabling enhanced photocatalytic CO<sub>2</sub> reduction in a gas-solid system without additives**

*Rui-Gang Yang,<sup>a</sup> Yao-Mei Fu,<sup>b</sup> Xing Meng,<sup>a</sup> Li Xue,<sup>a</sup> Zhen Zhou,<sup>a</sup> Yu-Ou He,<sup>a</sup> Jian-Xin*

*Qu,<sup>a</sup> Hai-Ning Wang,<sup>\*a</sup> and Zhong-Min Su,<sup>b,c</sup>*

<sup>a</sup>School of Chemistry and Chemical Engineering, Shandong University of Technology, Zibo 255049, People's Republic of China. E-mail: wanghn913@foxmail.com, mengxing837@foxmail.com.

<sup>b</sup>Shandong Engineering Research Center of Green and High-value Marine Fine Chemical; Weifang University of Science and Technology, Shouguang, 262700, China.

<sup>c</sup>School of Chemistry and Environmental Engineering, Changchun University of Science and Technology, Changchun, 130022, China.

## 1. Reagents and solvents

square acid, titanium (IV) isopropoxide, 1,3,5-triformylphloroglucinol (Tp), 1,4-phenylenediamine (Pa), isopropyl alcohol, mesitylene, 1,4-dioxane, acetic acid, ethanol, 5% Nafion solution, sodium sulfate, tetrahydrofuran, acetone. All the above reagents are purchased from Macleans Biochemical Co., Ltd (Shanghai).

## 2. Material characterization

The FTIR-850 is applied to record the Fourier transform infrared spectra (FT-IR) of the samples. The apparent morphology of the samples is analyzed via scanning electron microscopy (SEM, Sirion 200) at an accelerating voltage of 20 kV. The X-ray photoelectron spectroscopy (XPS) measurements are conducted on a scanning X-ray microprobe (K-Alpha, Thermo Scientific), which used Al  $\alpha$  radiation and the C 1s peak at 284.8 eV as an internal standard. The ultraviolet-visible (UV-Vis) spectra of the samples are tested using a UV-2550 spectrophotometer from Shimadzu, Japan. The CO<sub>2</sub> adsorption/desorption experiment (BSD-PM2) is carried out at 298 K.

## 3. Photocurrent measurements

The electrochemical analysis was carried out by the electrochemical analyzer (CHI 760E), using a standard three-electrode system for photocurrent response test and Mott-Schottky test. The electrolyte solution is 0.2 mol·L<sup>-1</sup> sodium sulfate solution, Ag/AgCl electrode is used as reference electrode, platinum electrode is used as counter electrode, and ITO glass coated with photocatalyst is used as working electrode. The working electrode was prepared by adding photocatalyst (1 mg) and 5% Nafion (10  $\mu$ L) to 1 mL ethanol and ultrasonic treatment for 1 h, and then dripping the resulting suspension on 1 cm  $\times$  2 cm ITO glass.

## 4. Photocatalytic measurements

Disperse the synthesized sample (2 mg) in 1 mL ethanol for 30 minutes to make it uniformly distribution, and then drip it on a 1 cm  $\times$  3 cm glass slide with a coverage area of 1 cm  $\times$  3 cm, which was heated at 100 °C to remove the ethanol. The prepared sample was placed in a self-made photocatalytic reactor, and about 100  $\mu$ L of deionized water was added to the bottom as a reducing agent. The CO<sub>2</sub> with different concentrations was used to replace the air inside the reactor and full of the reactor. The LED lamp was used as the light source and irradiated the sample for 2 h. 0.5 mL and 1.0 mL of the photocatalyzed mixed gas were injected into the gas chromatograph (GC 1120) to determine the CO content in the gas respectively.

## 5. Synthesis of TpPa-1

**TpPa-1** was synthesized on the basis of the reported literature<sup>1</sup>. Firstly, Tp (63 mg, 0.3 mmol) and Pa (48 mg, 0.45 mmol) were added into the glass tube. Secondly, 1.0 mL of mesitylene and 3.0 mL of 1,4-dioxane were introduced into the glass tube. Thirdly, the mixture was treated via the ultrasound method for 30 min. Fourthly, the resulting mixed system was rapidly frozen in liquid nitrogen bath (77K), degassed by three freeze-pump-thaw cycles, and sealed under vacuum after the addition of the acetic acid solution (6 M, 0.4 mL). Finally, the resulting system was heated at 120°C for 72 h, and then cooled to room temperature. The obtained product was separately extracted in tetrahydrofuran and acetone solutions for 24 h respectively, and then dried in vacuum

to obtain the red powder.

## 6. Synthesis of IEF-11

The synthesis of **IEF-11** was based on a slight modification of the already reported literature<sup>2</sup>. 255 mg (2.24 mmol) of square acid was placed in the liner of a polytetrafluoroethylene reactor, to which 8.2 mL (0.7 mmol) of isopropanol solution was added and sonicated for 5 min to completely dissolve it, then 6.4 mL (111.9 mmol) of glacial acetic acid was added to it and sonicated for 15 min, and finally 762  $\mu$ L of tetraisopropyl titanate was added to the reaction system, heating at 120°C for 48 h. The orange product was washed with isopropanol, filtered and dried, and collected.

## 7. Synthesis of TpPa@IEF-X series photocatalyst

**TpPa-1** and 26 mg of square acid with certain masses (50 mg, 100 mg and 150 mg, respectively) were added to the polytetrafluoroethylene reactor liner containing 8.2 ml of isopropanol solution and sonicated for 5 min until they dissolved. 640  $\mu$ L of glacial acetic acid was added and sonicated for 15 min. 80  $\mu$ L of titanium isopropoxide solution was then slowly added and heated at 120°C for 48 h to obtain the **TpPa@IEF-X** series catalyst.

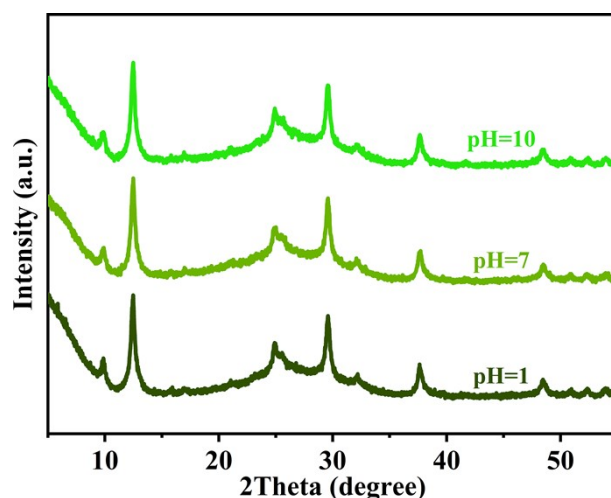


Fig. S1 XRD spectra of **TpPa@IEF-150** treated in different pH solutions.

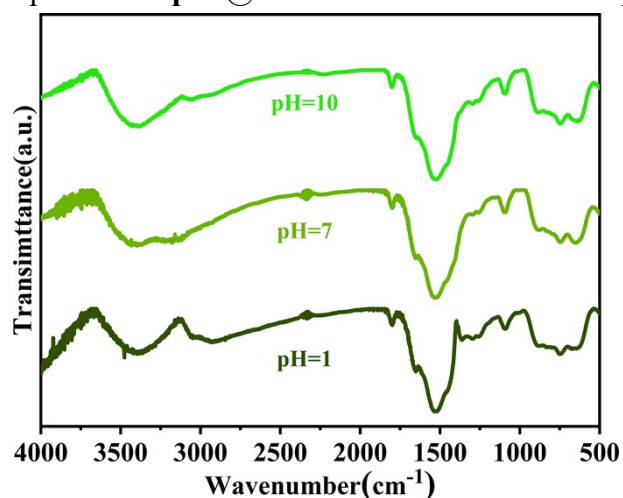


Fig. S2 FT-IR spectra of **TpPa@IEF-150** treated in different pH solutions.

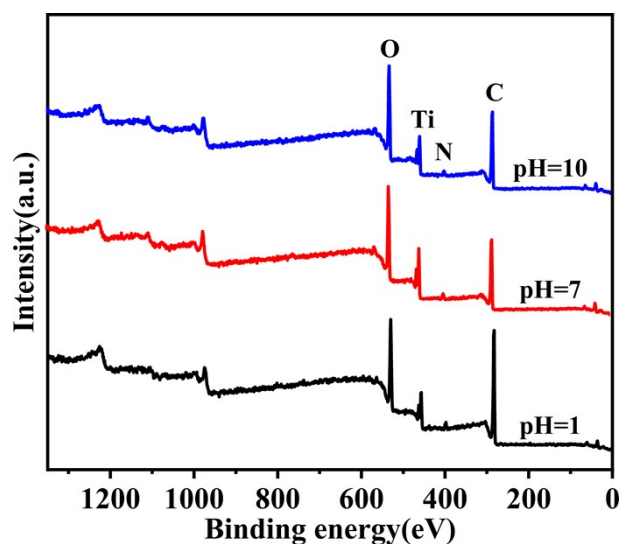


Fig. S3 XPS spectra of TpPa@IEF-150 treated in different pH solutions.

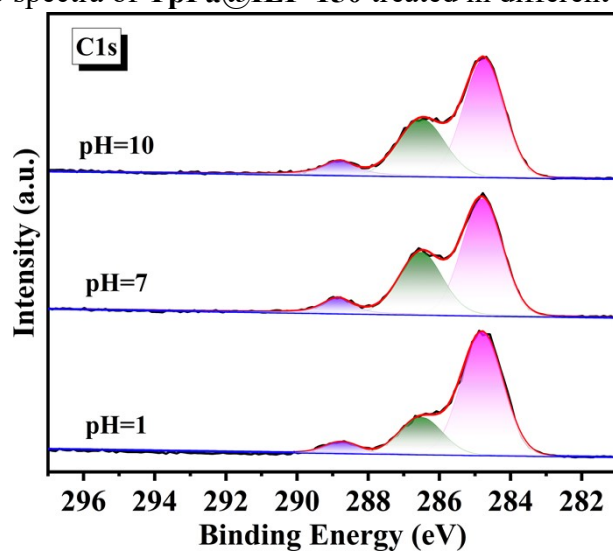


Fig. S4 High-resolution XPS spectra of C1s in TpPa@IEF-150 at different pH solutions.

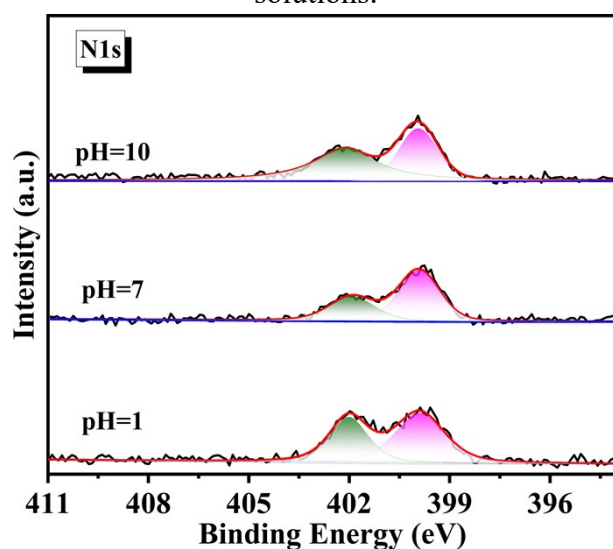
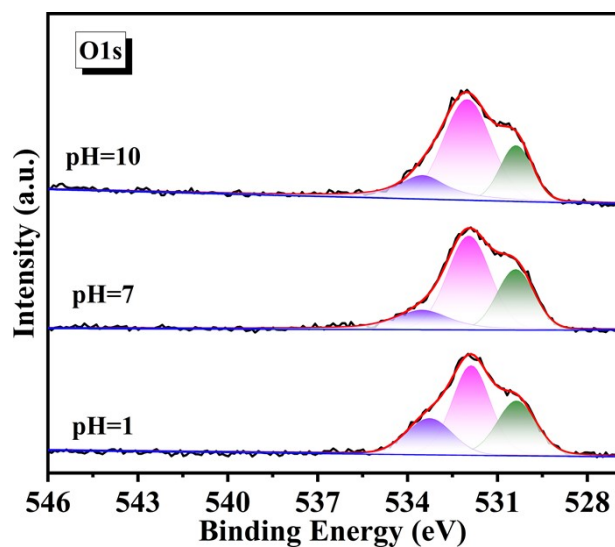
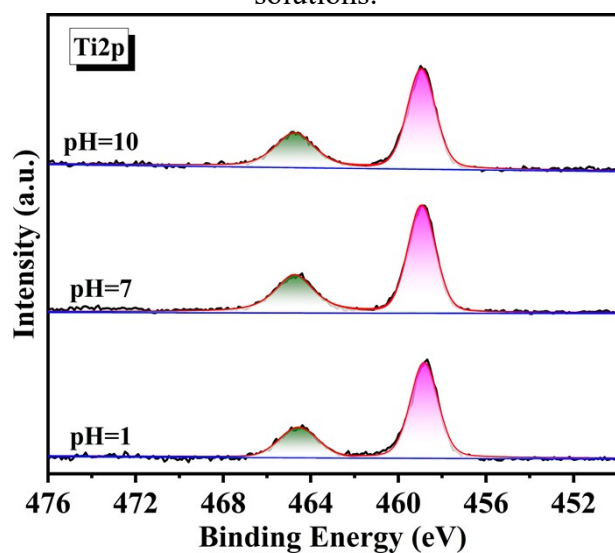


Fig. S5 High-resolution XPS spectra of N1s in TpPa@IEF-150 at different pH solutions.



**Fig. S6** High-resolution XPS spectra of O1s in **TpPa@IEF-150** at different pH solutions.



**Fig. S7** High-resolution XPS spectra of Ti2p in **TpPa@IEF-150** at different pH solutions.

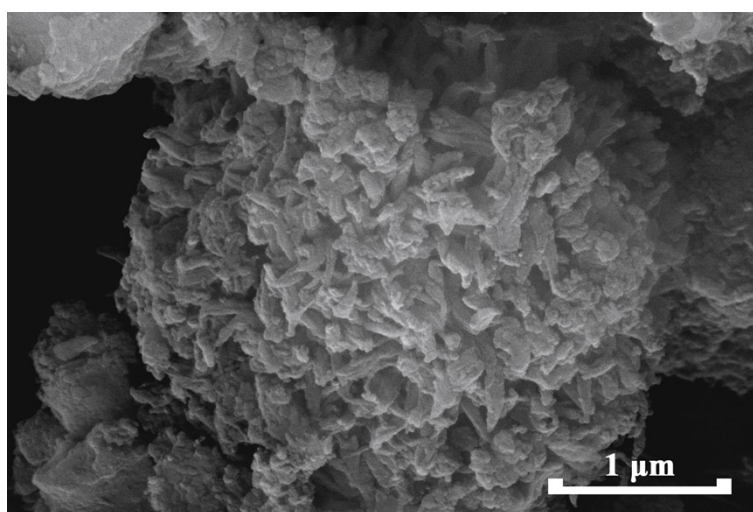


**Fig. S8** SEM images of **TpPa@IEF-150** after treatment in pH=1 solution.

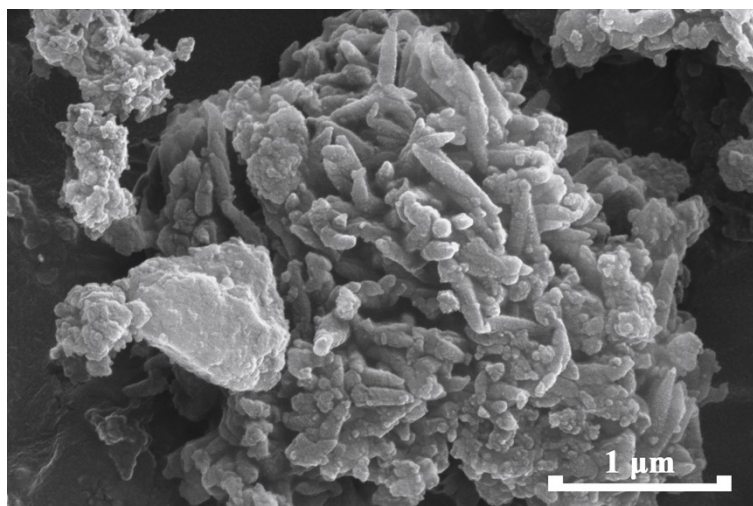


**Fig. S9** SEM images of **TpPa@IEF-150** after treatment in pH=7 solution.

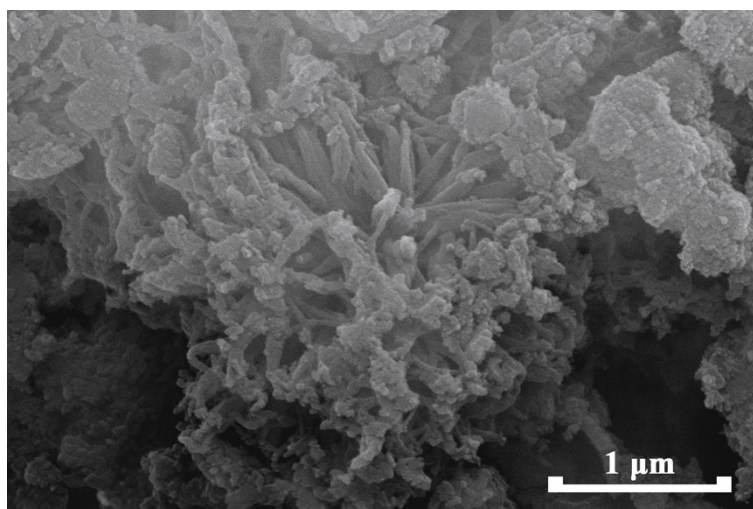


**Fig. S10** SEM images of **TpPa@IEF-150** after treatment in pH=10 solution.

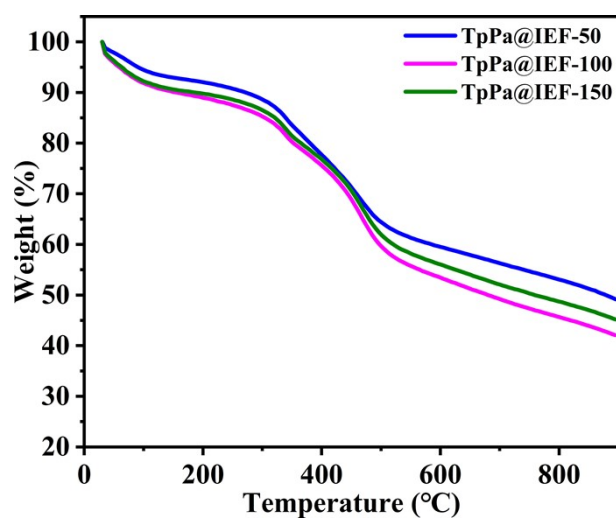


**Fig. S11** The TG curves of **TpPa@IEF-X**.

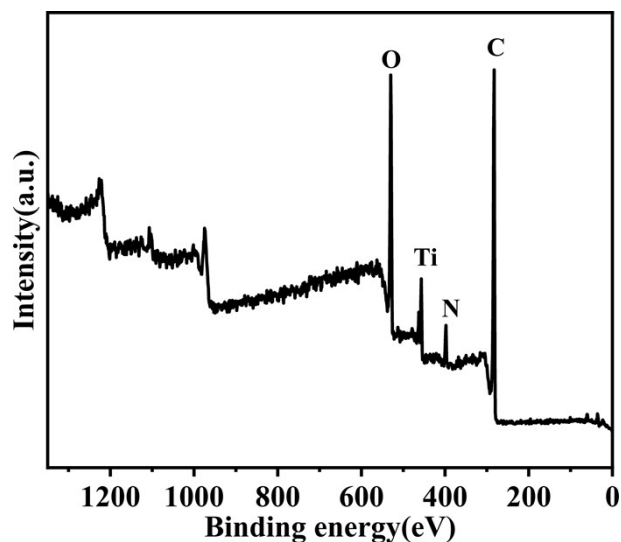


Fig. S12 XPS spectrum of TpPa@IEF-150.

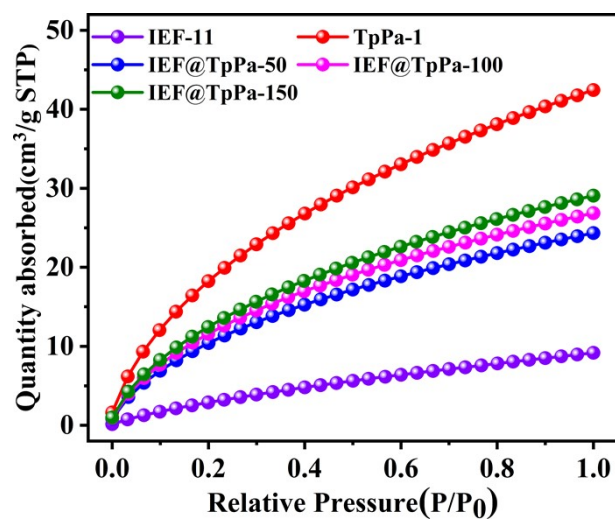


Fig. S13 CO<sub>2</sub> adsorption curves of TpPa-1, IEF-11 and TpPa@IEF-X.

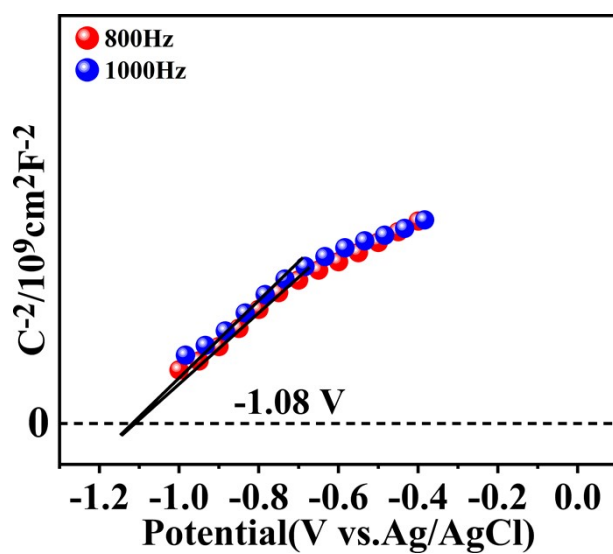


Fig. S14 Mott-Schottky curves of IEF-11.

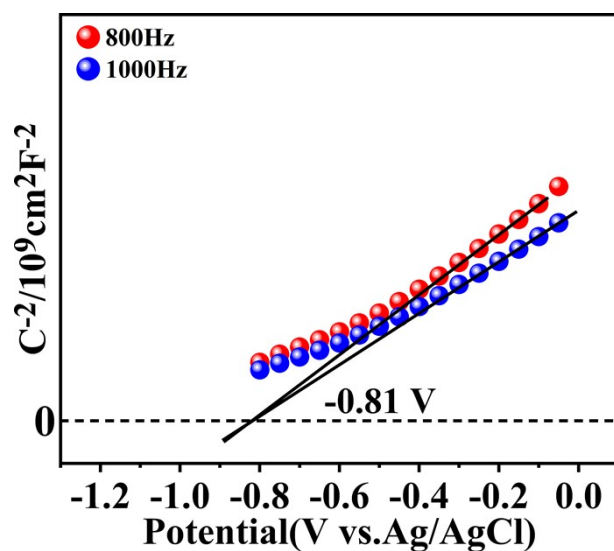


Fig. S15 Mott-Schottky curves of TpPa-1.

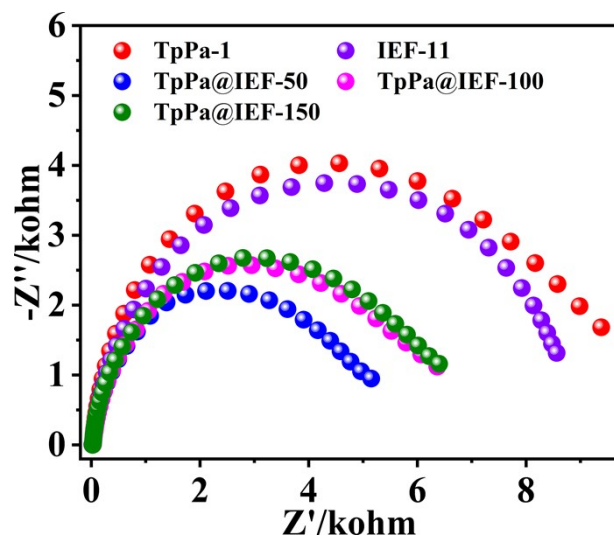


Fig. S16 Electrochemical impedance diagram of the photocatalysts.

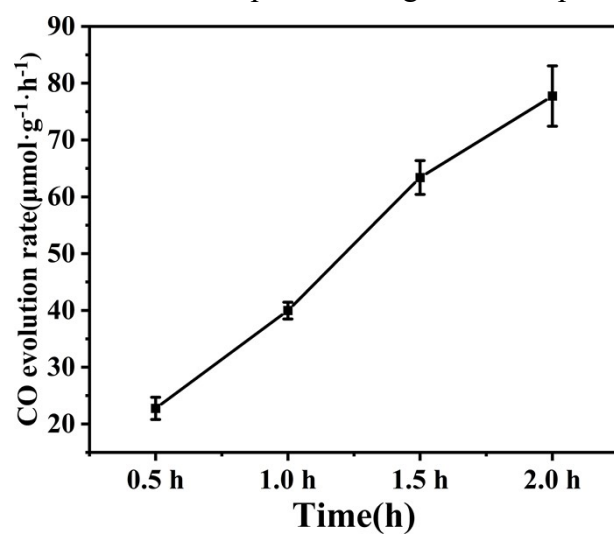
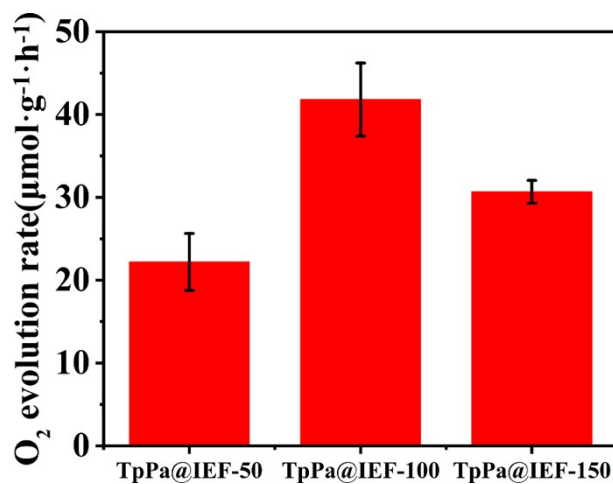
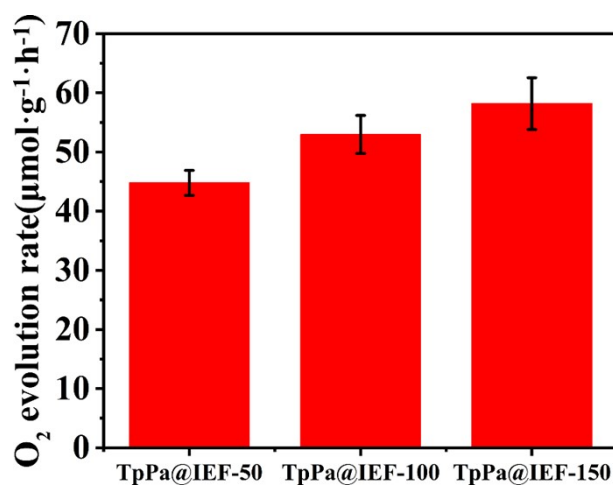


Fig. S17 The time-dependent formation rates of CO by TpPa@IEF-100.



**Fig. S18** O<sub>2</sub> evolution rates of the composite sample **TpPa@IEF-X** in 100% CO<sub>2</sub> environment.



**Fig. S19** O<sub>2</sub> evolution rates of the composite sample **TpPa@IEF-X** in 10% CO<sub>2</sub> environment.

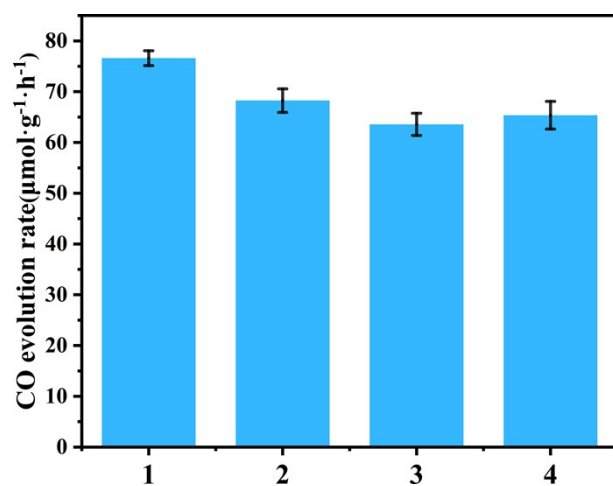


**Fig. S20** The durability in pure CO<sub>2</sub> environment by **TpPa@IEF-100**.

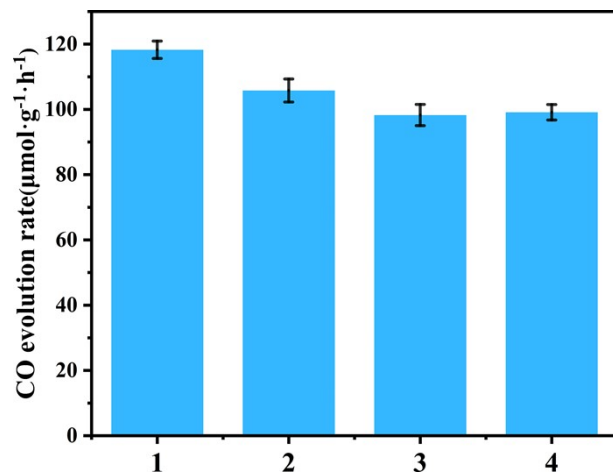


**Fig. S21** The durability in dilute CO<sub>2</sub> environment by **TpPa@IEF-150**.

**Tab. S1** The selectivity of catalytic products of composite samples in different CO<sub>2</sub> concentration environments

| Photocatalyst | CO Selectivity                                 |
|---------------|--|
| IEF-TpPa-50   | 98% (100% CO <sub>2</sub> )                    |
| IEF-TpPa-100  | 96% (100% CO <sub>2</sub> )                    |
| IEF-TpPa-150  | 97% (100% CO <sub>2</sub> )                    |
| IEF-TpPa-50   | 91% (10% CO <sub>2</sub> +90% N <sub>2</sub> ) |
| IEF-TpPa-100  | 98% (10% CO <sub>2</sub> +90% N <sub>2</sub> ) |
| IEF-TpPa-150  | 96% (10% CO <sub>2</sub> +90% N <sub>2</sub> ) |

**Tab. S2** Summary of photocatalytic CO<sub>2</sub> reduction work.

| Photocatalyst   | Products (μmol·g <sup>-1</sup> ·h <sup>-1</sup> ) | Reaction agent   | Ref        |
|---|---|------------------|------------|
| CT-COF  | CO (102.70)                                       | H <sub>2</sub> O | <b>S3</b>  |
| MTCN-H(ys)  | CO (18.12)  | H <sub>2</sub> O | <b>S4</b>  |
| TTCOF-Zn  | CO (2.06)   | H <sub>2</sub> O | <b>S5</b>  |
| SnS <sub>2</sub> /S-CTFs  | CO (123.60)<br>CH <sub>4</sub> (43.40)            | TEOA             | <b>S6</b>  |
| α-Fe <sub>2</sub> O <sub>3</sub> /g-C <sub>3</sub> N <sub>4</sub> | CO (27.20)  | H <sub>2</sub> O | <b>S7</b>  |
| C-TiO <sub>2-x</sub> /g-C <sub>3</sub> N <sub>4</sub>             | CO (204.96)                                       | H <sub>2</sub> O | <b>S8</b>  |
| COF-318-TiO <sub>2</sub>  | CO (69.67)  | H <sub>2</sub> O | <b>S9</b>  |
| In-MOF@TP-TA  | CO (25.00)<br>CH <sub>4</sub> (11.67)             | H <sub>2</sub> O | <b>S10</b> |
| NAHN-Tp/[Ir-ppy]  | CO (88.60)  | H <sub>2</sub> O | <b>S11</b> |
| g-C <sub>3</sub> N <sub>4</sub> (NH)/COF                          | CO (11.25)  | TEOA             | <b>S12</b> |
| TpPa/rGO  | CO (~200)   | TEOA             | <b>S13</b> |
| TiO <sub>2</sub> /TpPa  | CO (11.60)  | TEOA             | <b>S14</b> |
| TTCOF-MnMo <sub>6</sub>   | CO (37.25)  | H <sub>2</sub> O | <b>S15</b> |
| TTCOF/NUZ(UiO-66-NH <sub>2</sub> )                                | CO (6.56)   | H <sub>2</sub> O | <b>S16</b> |

## References

1. J.-L. Sheng, H. Dong, X.-B. Meng, H.-L. Tang, Y.-H. Yao, D.-Q. Liu, L.-L. Bai, F.-M. Zhang, J.-Z. Wei and X.-J. Sun, Effect of Different Functional Groups on Photocatalytic Hydrogen Evolution in Covalent-Organic Frameworks, *ChemCatChem*, 2019, **11**, 2313-2319.
2. P. Salcedo-Abraira, A. A. Babaryk, E. Montero-Lanzuela, O. R. Contreras-Almengor, M. Cabrero-Antonino, E. S. Grape, T. Willhammar, S. Navalón, E. Elkäim, H. García and P. Horcajada, A Novel Porous Ti-Squarate as Efficient Photocatalyst in the Overall Water Splitting Reaction under Simulated Sunlight Irradiation, *Adv. Mater.*, 2021, **33**, 2106627.
3. K. Lei, D. Wang, L. Ye, M. Kou, Y. Deng, Z. Ma, L. Wang and Y. Kong, A Metal-Free Donor–Acceptor Covalent Organic Framework Photocatalyst for Visible-Light-Driven Reduction of CO<sub>2</sub> with H<sub>2</sub>O, *ChemSusChem*, 2020, **13**, 1725-1729.
4. M. Zhang, J.-N. Chang, Y. Chen, M. Lu, T.-Y. Yu, C. Jiang, S.-L. Li, Y.-P. Cai and Y.-Q. Lan, Controllable Synthesis of COFs-Based Multicomponent Nanocomposites from Core-Shell to Yolk-Shell and Hollow-Sphere Structure for Artificial Photosynthesis, *Adv. Mater.*, 2021, **33**, 2105002.
5. M. Lu, J. Liu, Q. Li, M. Zhang, M. Liu, J.-L. Wang, D.-Q. Yuan and Y.-Q. Lan, Rational Design of Crystalline Covalent Organic Frameworks for Efficient CO<sub>2</sub> Photoreduction with H<sub>2</sub>O, *Angew. Chem., Int. Ed.*, 2019, **58**, 12392-12397.
6. S. Guo, P. Yang, Y. Zhao, X. Yu, Y. Wu, H. Zhang, B. Yu, B. Han, M. W. George and Z. Liu, Direct Z-Scheme Heterojunction of SnS<sub>2</sub>/Sulfur-Bridged Covalent Triazine Frameworks for Visible-Light-Driven CO<sub>2</sub> Photoreduction, *ChemSusChem*, 2020, **13**, 6278-6283.
7. Z. Jiang, W. Wan, H. Li, S. Yuan, H. Zhao and P. K. Wong, A Hierarchical Z-Scheme  $\alpha$ -Fe<sub>2</sub>O<sub>3</sub>/g-C<sub>3</sub>N<sub>4</sub> Hybrid for Enhanced Photocatalytic CO<sub>2</sub> Reduction, *Adv. Mater.*, 2018, **30**, 1706108.
8. J. Zhou, H. Wu, C.-Y. Sun, C.-Y. Hu, X.-L. Wang, Z.-H. Kang and Z.-M. Su, Ultrasmall C-TiO<sub>2-x</sub> nanoparticle/g-C<sub>3</sub>N<sub>4</sub> composite for CO<sub>2</sub> photoreduction with high efficiency and selectivity, *J. Mater. Chem. A*, 2018, **6**, 21596-21604.
9. M. Zhang, M. Lu, Z.-L. Lang, J. Liu, M. Liu, J.-N. Chang, L.-Y. Li, L.-J. Shang, M. Wang, S.-L. Li and Y.-Q. Lan, Semiconductor/Covalent-Organic-Framework Z-Scheme Heterojunctions for Artificial Photosynthesis, *Angew. Chem., Int. Ed.*, 2020, **59**, 6500-6506.
10. L. Wang, J. Mao, G. Huang, Y. Zhang, J. Huang, H. She, C. Liu, H. Liu and Q. Wang, Configuration of hetero-framework via integrating MOF and triazine-containing COF for charge-transfer promotion in photocatalytic CO<sub>2</sub> reduction, *Chem. Eng. J.*, 2022, **446**, 137011.
11. S.-Q. You, J. Zhou, M.-M. Chen, C.-Y. Sun, X.-J. Qi, A. Yousaf, X.-L. Wang and Z.-M. Su, A hydrazone-based covalent organic framework/iridium (III) complex for photochemical CO<sub>2</sub> reduction with enhanced efficiency and durability, *Journal of Catalysis*, 2020, **392**, 49-55.

12. J. Wang, Y. Yu, J. Cui, X. Li, Y. Zhang, C. Wang, X. Yu and J. Ye, Defective g-C<sub>3</sub>N<sub>4</sub>/covalent organic framework van der Waals heterojunction toward highly efficient S-scheme CO<sub>2</sub> photoreduction, *Appl. Catal., B*, 2022, **301**, 120814.
13. V. N. Gopalakrishnan, D.-T. Nguyen, J. Becerra, M. Sakar, J. M. E. Ahad, J. J. Jautzy, L. M. Mindorff, F. Béland and T.-O. Do, Manifestation of an Enhanced Photoreduction of CO<sub>2</sub> to CO over the In Situ Synthesized rGO–Covalent Organic Framework under Visible Light Irradiation, *ACS Applied Energy Materials*, 2021, **4**, 6005-6014.
14. X. An, J. Bian, K. Zhu, R. Liu, H. Liu and J. Qu, Facet-dependent activity of TiO<sub>2</sub>/covalent organic framework S-scheme heterostructures for CO<sub>2</sub> photoreduction, *Chem. Eng. J.*, 2022, **442**, 135279.
15. M. Lu, M. Zhang, J. Liu, T.-Y. Yu, J.-N. Chang, L.-J. Shang, S.-L. Li and Y.-Q. Lan, Confining and Highly Dispersing Single Polyoxometalate Clusters in Covalent Organic Frameworks by Covalent Linkages for CO<sub>2</sub> Photoreduction, *J. Am. Chem. Soc.*, 2022, **144**, 1861-1871.
16. Q. Niu, S. Dong, J. Tian, G. Huang, J. Bi and L. Wu, Rational Design of Novel COF/MOF S-Scheme Heterojunction Photocatalyst for Boosting CO<sub>2</sub> Reduction at Gas–Solid Interface, *ACS Appl. Mater. Interfaces*, 2022, **14**, 24299-24308.